Research Article | Vol. 6, No. 9 | 1 Sep 2016 | OPTICAL MATERIALS EXPRESS 2947

Optical Materials EXPRESS

Vapor deposited Cr-doped ZnS thin films: towards optically pumped mid-infrared waveguide lasers

ERIC A. KARHU,[1] CHARLES R. ILDSTAD,[1] STEFANO POGGIO,[2] VEDRAN FURTULA,[1] NIKOLAI TOLSTIK,[1] IRINA T. SOROKINA,[1] JOSEPH J. BELBRUNO,[2] AND URSULA J. GIBSON[1,2,*]

[1]*Department of Physics, Norwegian University of Science and Technology, N-7491 Trondheim, Norway*
[2]*Department of Chemistry, Dartmouth College, Hanover, NH, 03755-6128, USA*
**ursula.gibson@ntnu.no*

Abstract: Compact, affordable mid-IR lasers require the development of gain materials in waveguide form. We report on the high vacuum deposition of Cr:ZnS films with concentration ranging from 10^{18}-10^{20} dopants/cm^3 . At low concentrations, films display well-isolated absorption associated with substitutional Cr^{2+} ions in the lattice. Spatial modulation of the dopant concentration suppresses the absorption associated with this substitution. Lateral crystallite sizes less than 30 nm are associated with the lowest substrate temperatures (<50 °C) used during deposition, and waveguide losses as low as 8dB/cm are observed. These materials are promising candidates as gain media for fabrication of waveguide mid-IR lasers.

OCIS codes: (160.4760) Optical properties; (240.0310) Thin films.

References and links

1. I. T. Sorokina and E. Sorokin, "Femtosecond Cr^{2+}-Based Lasers," IEEE J. Sel. Top. Quantum Electron. **21**(1), 1601519 (2015).
2. C. Kim, D. V. Martyshkin, V. V. Fedorov, and S. B. Mirov, "Middle-infrared random lasing of Cr^{2+} doped ZnSe, ZnS, CdSe powders, powders imbedded in polymer liquid solutions, and polymer films," Opt. Commun. **282**(10), 2049–2052 (2009).
3. D. V. Martyshkin, V. V. Fedorov, C. Kim, I. S. Moskalev, and S. B. Mirov, "Mid-IR random lasing of Cr-doped ZnS nanocrystals," J. Opt. **12**(2), 24005 (2010).
4. S. Mirov, V. Fedorov, I. Moskalev, M. Mirov, and D. Martyshkin, "Frontiers of mid-infrared lasers based on transition metal doped II–VI semiconductors," J. Lumin. **133**, 268–275 (2013).
5. S. Wang, S. B. Mirov, V. V. Fedorov, and R. P. Camata, "Synthesis and spectroscopic properties of Cr doped ZnS crystalline thin films," in *Solid State Lasers Xiii: Technology and Devices*, R. Scheps and H. J. Hoffman, eds. (Spie-Int Soc Optical Engineering, 2004), Vol. 5332, pp. 13–20.
6. J. R. Macdonald, S. J. Beecher, A. Lancaster, P. A. Berry, K. L. Schepler, S. B. Mirov, and A. K. Kar, "Compact Cr:ZnS channel waveguide laser operating at 2,333 nm," Opt. Express **22**(6), 7052–7057 (2014).
7. N. A. Vlasenko, P. F. Oleksenko, M. A. Mukhlyo, Z. L. Denisova, and L. I. Veligura, "ZnS:Cr and ZnSe:Cr thin-film waveguide structures as electrically pumped laser media with an impact excitation mechanism," Ann. Phys. **525**(12), 889–905 (2013).
8. M. Nematollahi, X. Yang, L. M. S. Aas, Z. Ghadyani, M. Kildemo, U. J. Gibson, and T. W. Reenaas, "Molecular beam and pulsed laser deposition of ZnS:Cr for intermediate band solar cells," Sol. Energy Mater. Sol. Cells **141**, 322–330 (2015).
9. J. E. Williams, R. P. Camata, V. V. Fedorov, and S. B. Mirov, "Pulsed laser deposition of chromium-doped zinc selenide thin films for mid-infrared applications," Appl. Phys. - Mater. Sci. Process. **91**(2), 333–335 (2008).
10. I. P. McClean and C. B. Thomas, "Photoluminescence study of MBE-grown films on ZnS," Semicond. Sci. Technol. **7**(11), 1394–1399 (1992).
11. M. C. Morris, H. F. McMurdie, E. H. Evans, B. Paretzkin, J. H. de Groot, C. R. Hubbard, and S. J. Carmel, *Standard X-Ray Diffraction Powder Patterns: - 13- Data for 58 Substances* (National Bureau of Standards, 1976), Vol. #00–027–1402.
12. T. Huang, W. Parrish, N. Masciocchi, and P. Wang, in *Advances in X-Ray Analysis - Volume 33 | Charles S. Barrett | Springer* (n.d.), Vol. 33, p. 295.
13. J. Topolancik, F. Vollmer, R. Ilic, and M. Crescimanno, "Out-of-plane scattering from vertically asymmetric photonic crystal slab waveguides with in-plane disorder," Opt. Express **17**(15), 12470–12480 (2009).
14. M. D. Himel and U. J. Gibson, "Measurement of planar waveguide losses using a coherent fiber bundle," Appl. Opt. **25**(23), 4413 (1986).

#272176 http://dx.doi.org/10.1364/OME.6.002947
Journal © 2016 Received 22 Jul 2016; revised 17 Aug 2016; accepted 17 Aug 2016; published 23 Aug 2016

Optical Materials EXPRESS

15. I. T. Sorokina, E. Sorokin, S. Mirov, V. Fedorov, V. Badikov, V. Panyutin, and K. I. Schaffers, "Broadly tunable compact continuous-wave Cr(2+):ZnS laser," Opt. Lett. **27**(12), 1040–1042 (2002).
16. M. Chen, C. Hu, W. Li, H. Kou, J. Li, Y. Pan, and B. Jiang, "Cr3+ in diffusion doped Cr^{2+}:ZnS," Ceram. Int. **40**(5), 7573–7577 (2014).
17. V. Y. Ivanov, Y. G. Semenov, M. Surma, and M. Godlewski, "On the nature of the anti-Stokes luminescence in chromium-doped ZnSe crystals," J. Lumin. **72–4**, 101–102 (1997).
18. J. Peppers, V. V. Fedorov, and S. B. Mirov, "Mid-IR photoluminescence of Fe^{2+} and Cr^{2+} ions in ZnSe crystal under excitation in charge transfer bands," Opt. Express **23**(4), 4406–4414 (2015).
19. R. Swanepoel, "Determination of the Thickness and Optical-Constants of Amorphous-Silicon," J. Phys. E Sci. Instrum. **16**(12), 1214–1222 (1983).
20. D. Minkov and R. Swanepoel, "Computerization of the Optical Characterization of a Thin Dielectric Film," Opt. Eng. **32**(12), 3333–3337 (1993).
21. S. B. Mirov, V. V. Fedorov, K. Graham, I. S. Moskalev, I. T. Sorokina, E. Sorokin, V. Gapontsev, D. Gapontsev, V. V. Badikov, and V. Panyutin, "Diode and fibre pumped Cr^{2+}:ZnS mid-infrared external cavity and microchip lasers," IEEE Proc. - Optoelectron. **150**, 340–345 (2003).
22. E. Karhu, N. Tolstik, E. Sorokin, S. Polyakov, R. Zamiri, V. Furtula, U. Osterberg, I. T. Sorokina, and U. J. Gibson, "Towards Mid-IR Waveguide Lasers: Transition Metal Doped ZnS Thin Films," in (OSA, 2016), p. STu4R.2.
23. N. Tolstik, E. Sorokin, E. A. Karhu, S. Polyakov, U. J. Gibson, and I. T. Sorokina, "MBE-grown Cr:ZnS Thin Film Laser Media," in (OSA, 2016), p. JFK1.5.
24. S. Schön, M. Chaichimansour, W. Park, E. W. Thomas, T. Yang, B. K. Wagner, and C. J. Summers, "Improved photoluminescent properties of ZnS: Mn due to the δ-doping process," J. Soc. Inf. Disp. **6**(1), 67–71 (1998).
25. M. D. Himel, J. A. Ruffner, and U. J. Gibson, "Stress modification and reduced waveguide losses in ZnS thin films," Appl. Opt. **27**(14), 2810–2811 (1988).
26. J. A. Ruffner, M. D. Himel, V. Mizrahi, G. L. Stegeman, and U. J. Gibson, "Effects of low substrate temperature and ion assisted deposition on composition, optical properties, and stress of ZnS thin films," Appl. Opt. **28**(24), 5209–5214 (1989).
27. H. Nelkowski and G. Grebe, "IR-luminescence of ZnS:Cr," J. Lumin. **1**, 88–93 (1970).
28. E. Seim, "TEM characterization of Cr-doped ZnS Thin Films for Solar Cell applications; http://urn.kb.se/resolve?urn=urn:nbn:no:ntnu:diva-25057," MS thesis, Norwegian Univ. of Sci & Technol (2014).
29. N.-A. Molland, Z. Ghadyani, E. A. Karhu, S. Poggio, M. Nematollahi, M. Kildemo, T. W. Reenaas, J. J. BelBruno, and U. J. Gibson, "Band-edge modification and mid-infrared absorption of co-deposited Fe_xZn_1-xS thin films," Opt. Mater. Express **5**(7), 1613 (2015).
30. E. J. Baerends, E. Baerends, "Precise Density-Functional Method for Periodic Structures," Phys. Rev. B Condens. Matter **44**(15), 7888–7903 (1991).
31. S. Vosko, L. Wilk, and M. Nusair, "Accurate Spin-Dependent Electron Liquid Correlation Energies for Local Spin-Density Calculations - a Critical Analysis," Can. J. Phys. **58**(8), 1200–1211 (1980).
32. J. P. Perdew, K. Burke, and M. Ernzerhof, "Generalized gradient approximation made simple," Phys. Rev. Lett. **77**(18), 3865–3868 (1996).

1. Introduction

Improved spectroscopic techniques and the demonstration of high power mid-infrared sources suitable for the production of frequency combs are driving an increasing interest in transition-metal-doped chalcogenide lasers. Of the materials studied to date for application in the 2-3.5 μm band, Cr:ZnS stands out as an excellent candidate for further development [1]. For applications from sensing to medical diagnostics and surgery, a compact source is desired, and development of alternatives to single-crystal gain media have been pursued for several years [2–5]. Successful lasing in a waveguide configuration has been achieved when femtosecond pulses were used to define a channel within a single crystal [6], and laser oscillations were reported using impact ionization of a thin film [7]. In the latter case, significant degradation of the material was reported after operation. Pulsed laser deposition of Cr:ZnS and Cr:ZnSe has been reported [5,8,9], with significant variation in optical properties. Co-deposition of Mn during molecular beam epitaxy of ZnS has been shown to suppress S-related defects [10], suggesting that this deposition technique may be favorable for the deposition of other transition metal doped Zn chalcogenides.

In order to get high efficiency from an optically pumped device, a low concentration of Cr is required to prevent concentration quenching. There should be no parasitic absorption in the vicinity of the Cr^{2+} peak, and no other ionization states of the metal should be present. Additionally, long fluorescence lifetimes are desired and waveguide losses should be

Optical Materials EXPRESS

minimized. In this work, we demonstrate that films deposited under ultrahigh vacuum (UHV) at room temperature are promising materials for mid-IR waveguide laser development, and demonstrate that the crystalline grain size in the films is related to both overall Cr concentration and to flux variations.

2. Experimental methods

Cr-doped ZnS films were deposited onto single crystal (100) silicon, single crystal silicon with a 1 μm SiO_2 coating, CaF_2, and c-plane sapphire substrates in a chamber with a base pressure of 6 x 10^{-7} Pa. The CaF_2 substrates allowed extended range transmission measurements, but suffered adhesion failure over a period of weeks to months, sapphire substrates provided IR transparency and had good adhesion properties, the silicon substrates provided low background signal for X-ray diffraction, and the oxidized silicon substrates were used for waveguide loss measurements. The source materials used were Cr (99.996% metals basis) obtained from Alfa Aesar, Cr (99.999% metals basis) obtained from ESPI metals, and ZnS (99.995%) obtained from Alfa Aesar. The Cr metal was e-beam evaporated and ZnS was evaporated from a Knudsen cell. As measured by crystal oscillators (Inficon SQM-160 thin film deposition monitor) the deposition rates for Cr varied between 0.001 and 0.2 Å/s and between 7.8 and 18.5 Å/s for ZnS. An additional calibrated crystal monitor was placed close to the Cr source in order to measure the flux rate for films with the lowest Cr concentrations. Films were also made with a modulated doping, where the shutter was open for either 10% or 25% of the deposition, with 90 layers each of Cr-doped and pure ZnS. For the 10% duty cycle, the thicknesses of the individual layers were ~6.7 nm doped and 60 nm undoped; for the 25% film, the thicknesses were ~12.8 nm and 38 nm.

The substrates were degreased in acetone and isopropanol ultrasonic baths for 10 minutes each, blown dry with nitrogen, attached to a 10 cm stainless steel plate and immediately loaded into the vacuum chamber loadlock. The substrate holder was rotated at 25 rpm and films were deposited on either unheated (RT) substrates or on substrates heated to 200 °C (ET) using an infrared lamp. Selected films deposited on RT substrates were heated in situ after deposition to 400 °C for 12 hours (RTA).

The films were characterized by X-ray diffraction (XRD) using a Siemens D5500 diffractometer equipped with a focusing primary monochromator and 2.5° Soller slits. The peak positions were measured with respect to the Si(004) peak at 69.2° as a reference [11] on the Si(100) substrates and the Al_2O_3(006) peak at 41.71 ° [12] on the sapphire substrates.

Compositions of the films were determined using energy dispersive X-ray spectroscopy (EDX) performed in a Hitachi TM3000 electron microscope. For films with less than 0.1at% of Cr, atomic percentages were estimated from the flux rates of ZnS and Cr relative to those at films whose concentrations could be measured directly. The film thickness was measured by profilometry (Tencor Alphastep). Optical transmission measurements were performed from λ = 250 nm to 10 μm using a conventional spectrometer (OLIS 14) and an FTIR (Bruker Tensor 27).

Waveguide loss measurements were made with a Q-Photonics 40 mW laser diode at λ = 1060 nm delivered through a single mode telecom fiber by butt-coupling into the film, and measuring the out-of-plane scatter as a function of distance in the propagation direction. Butt-coupling was used so that a diode at λ = 650 nm and an optical microscope could be used to confirm good coupling before switching to the infrared diode, but had the disadvantage that individual mode selection was not possible. The method is similar to that of Topolancik [13], except that a scanned fiber is used instead of an IR camera. A fiber-coupled lens with a 4.3mm focal length was scanned in a 2-d grid over the sample, and the intensity was recorded using a lock-in amplifier and a Ge detector attached to the far end of the fiber, creating a map similar to that from an image-forming fiber bundle [14]. The peak intensity as a function of distance from the coupling point was used to derive a value of the losses, averaged over all modes excited in the films.

Optical Materials EXPRESS

3. Results and discussion

As determined by EDX, films had concentrations from 0.025 to 2.7 at% Cr, where the lowest values were extrapolated using relative deposition rates. The (Zn + Cr):S ratio was1 ± 0.03 for all films. Film thicknesses were between 1 - 12 µm.

3.1 Optical absorption

For Cr:ZnS, when Cr substitutes for Zn, crystal field splitting gives broad absorption and emission bands suitable for broadband mid-IR lasers [15]. Films with high concentrations of Cr show significant absorption associated with the inclusion of the transition metal within the ZnS host. The desired substitutional Cr^{2+} state has an absorption centered at ~0.77 eV, and there is additional parasitic absorption peak (labeled 'P' in Fig. 1) centered at ~2eV. The parasitic absorption, which has been separately attributed to Cr^{3+} in octahedral sites [16] and to photoionization of Cr^{2+} to Cr^{+}, by analogy to the behavior observed in ZnSe [17,18], is decreased when lower concentration films are made. The relative depth of the absorption peaks (relative to a linear baseline around each feature) is shown as a function of concentration in Fig. 1(b), indicating that concentrations less than ~0.2 at% are necessary to minimize the undesired parasitic absorption.

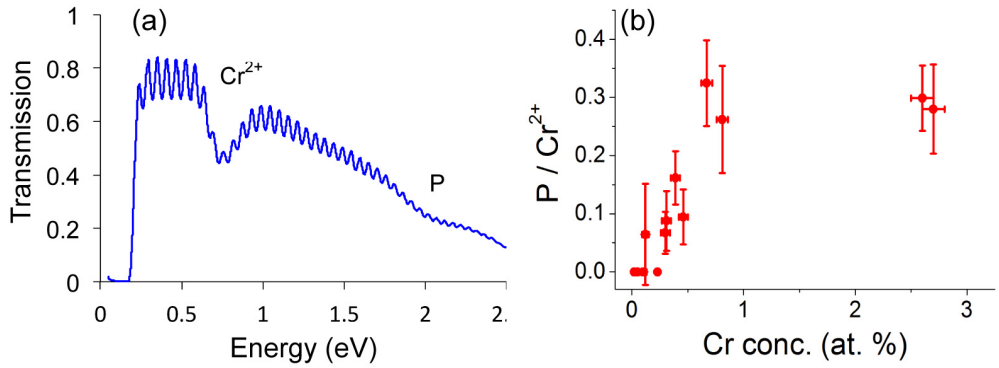

Fig. 1. (a) Transmission vs. energy for a film with 2.6 at% Cr deposited onto an unheated substrate. (b) Ratio of chromium absorption features as a function of concentration.

Transmission data is shown in Fig. 2(a) for three films with a Cr concentration of ~0.03 at% and thicknesses of 4-6 µm grown on sapphire substrates (transmission 86%) under different thermal conditions (RT - room temperature, RTA - room temperature annealed and ET-elevated temperature). The Cr^{2+} absorption is visible as a shallow dip near 1.6 µm. The films that were deposited at room temperature, whether or not annealed after deposition, had over 83% transmission from 0.7 to 4 µm with values approaching the bare substrate above 2 µm. Films deposited at 200 °C showed a rolloff in the transmission below 1.4 µm as did films with more than 0.46 at% Cr. The rolloff for the higher temperature depositions is most likely due to scatter, as the same effect is seen in pure ZnS films deposited onto heated substrates that also have increased surface roughness and crystallite size. Swanepoel analysis [19,20] was used to derive the thickness, index of refraction, and absorption of the films from the measured spectra. The index of refraction was slightly lower than bulk values from the literature (Fig. 2(b)), as expected due to the formation of voids in the thermally deposited thin films. The reduced index of the ET films, and published results on the structure of similar films [8] suggests that a significant portion of the loss is due to scattering from larger grains. Films with higher concentrations of Cr had slightly higher indices due to a higher packing fraction [8].

Optical Materials EXPRESS

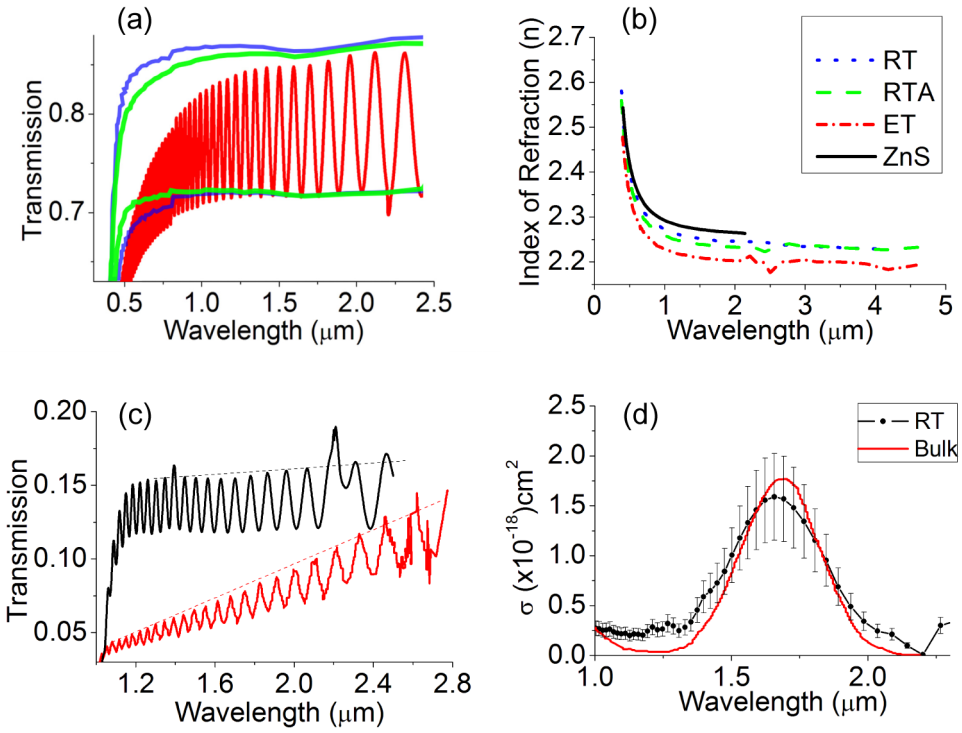

Fig. 2. (a) Envelope of the transmission curves for films grown without heating (blue - RT), deposited without heating, then annealed at 400 °C for 12 h(green - RTA) and full transmission curve for a film deposited at 200 °C (red curve - ET). Features at 800, 1400 and 2200 nm are artifacts from the spectrometer. (b) index of refraction for the same films, compared to bulk ZnS (c) comparison of infrared transmission for vacuum deposited (black line) and PLD (red line) [5] films on silicon (100) substrates d) Absorption cross-section for the Cr^{2+} ions in bulk Cr:ZnS [21], compared to the cross-section for absorption in the film, relative to the total concentration of Cr atoms in the film.

To compare the overall infrared performance to PLD films reported in [5], an 8.2 μm thick RT film with a Cr concentration ~1.4 x 10^{19} cm^{-3} (0.11 ± 0.03 at%) was grown and measured on a silicon (100) substrate (Fig. 2(c)). Comparatively little attenuation is observed between 2 μm to 1.2 μm in the thermally evaporated film, possibly due to the lower energy in this deposition process. (The features at 1.4 and 2.2 μm are from the spectrometer baseline).

For laser applications, the absorption cross-section ($\sigma = \alpha/N$, where α is the absorption coefficient and N is the ionic or atomic density) is an important figure of merit that indicates how much the Cr in the material contributes to the desired optical absorption. The cross-section is plotted in Fig. 2(d) for one of the films (black, atomic density) and compared to a single crystal sample (red) [21]. The atomic density is used for the film because the low sample volume makes analysis of ionization states difficult. The data thus represent a lower bound for the cross-section, as the density of C^{2+} will always be equal to, or less than, the atomic density. The peak cross-section is 1.79 x 10^{18} cm^2 at a wavelength of 1656 nm. The absorption peak is slightly broader for the RT deposited film compared to the crystal sample, but the values are very similar, suggesting that a high percentage of the Cr atoms in the film are in the desired substitutional (Cr^{2+}) state. Broadband fluorescence is observed in these films in the vicinity of 2 μm [22,23], demonstrating the potential for stimulated emission.

Optical Materials EXPRESS

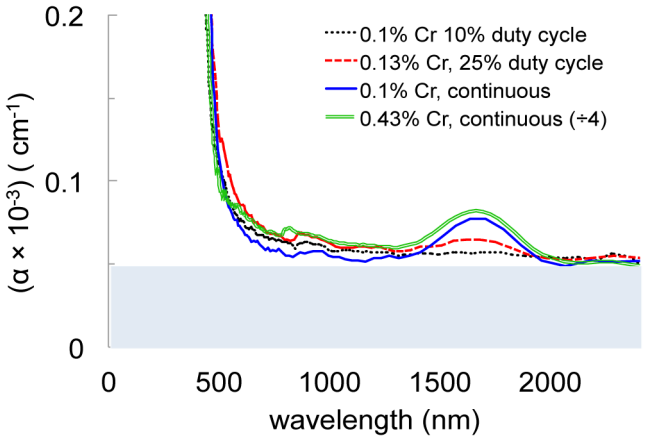

Fig. 3. Relative absorption of films deposited with continuous and modulated Cr fluxes. The modulated films (black dotted and red dashed curves) show little absorption from the Cr^{2+} ions relative to films with similar overall concentration deposited with a continuous Cr flux (blue curve). The double line (green) curve is the absorption of a film with a concentration similar to the peak value in the 25% duty cycle film, scaled down by a factor of four. The gray area indicates the region where the absolute accuracy is limited by the instrument; the offset of the curves was adjusted to make them coincide at 2500 nm.

Reports on modulated or delta-doping of Mn:ZnS indicate that variation of the transition metal ion concentrations in ZnS can have dramatic effects on the emission [24] and suggest that reduction of the dimensionality of the doped material can alter the fluorescence lifetime. We therefore compared films made with low Cr concentration with continuous metal deposition to those made with a time-varying Cr flux. Although this does not give individual atomic layers of Cr (true delta-doping), there is a large and reproduceable effect in the Cr^{2+} absorption. As seen in Fig. 3, the peak at 1600 nm is reduced for modulated films, and there is a slight shift in the absorption edge at short wavelengths. The shaded region represents the approximate floor of our measurement capability for α; vertical offsets were adjusted to make the absorption at 2500 nm coincide to make the comparison more clear. The red and black (dashed and dotted) curves are for films with an overall concentration of ~0.1 at%, made under two modulation conditions. The blue (single) curve presents the absorption for a film made with overall composition similar to the modulated films, and the green (double) curve gives the absorption values for a film with the same peak concentration as the 25% duty cycle film, normalized (divided by four) to account for the lower effective thickness of the Cr-containing regions. The change in the absorption does not appear to be attributable to either the peak concentration, or to the overall concentration. Two possibilities mechanisms that explain the reduction in the Cr^{2+} absorption are: a) enhanced interaction between Cr ions in the layered films, as is reported for Mn, or b) alterations in the crystal growth habit that limits the substitutional inclusion of Cr in the ZnS when the flux is modulated. Density functional theory calculations (section 4) for delta-doped layers do show the disappearance of the well-defined intra-gap states for monatomic layers of Cr in ZnS, but structural changes (section 3.3) are also observed. The absorption changes indicate that delta-doping is not a viable technique for increasing the lifetimes of the Cr:ZnS films reported here.

3.2 Waveguide loss measurements

Due to the difficulty of measuring small values of the attenuation coefficient, α, in transmission (perpendicular geometry), we assessed the losses by using films deposited on oxidized silicon substrates as waveguides, using the setup shown in Fig. 4(a). Figure 4(b) shows a two-dimensional map of the scattered intensity as a function of position, collected by a scanning fiber for the ET film shown in Fig. 2(a) and 2(b). The light was coupled in at an

Optical Materials EXPRESS

angle of ~15 degrees, so that the waveguide mode could be easily separated from light scattered across the top surface of the film. The waveguide mode therefore has an angle relative to the scan direction. Figure 4(c) shows the peak intensity vs. distance used to derive the value of the attenuation for this film. For the films that were heated during deposition, an attenuation coefficient of between 5 and 6 cm^{-1} was found, corresponding to 22-30 dB cm^{-1}. For films deposited onto unheated substrates, losses were as low as 8 dB cm^{-1}, comparable to literature reports on pure ZnS waveguides [25]. Films deposited on room temperature substrates, then heated after deposition (RTA) had losses comparable to the RT films that were not annealed.

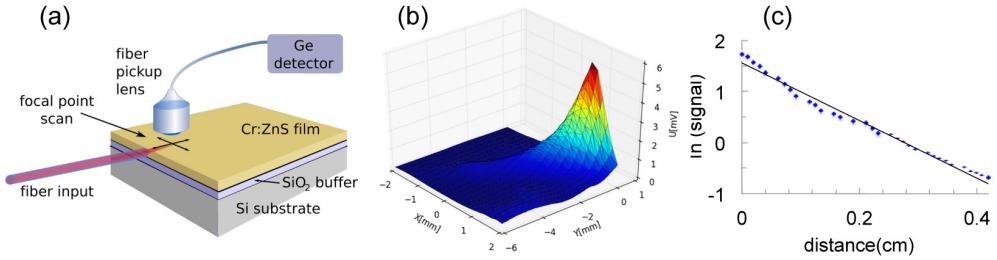

Fig. 4. (a) Schematic of measurement system, (b) 2-d scan of the intensity of scattered light from within the waveguide for the ET film shown in Fig. 2 and 3 (c) Plot of the natural log of the maximum intensity at each position along the length of the waveguide streak, along with an curve fit used to determine the attenuation.

With typical thicknesses of over 4 µm, and a high index contrast between both the silicon oxide layer on the substrate and the air above, the films formed multimode waveguides at the measurement wavelength (λ = 1060 nm). Since the higher order modes have higher losses, the results here represent an upper bound to losses that would be expected in single mode waveguides. The large thicknesses used for analysis of the fluorescence properties [22,23] result in greater surface roughness than would be expected in a film designed for single mode operation at 2 µm, increasing losses. The perpendicular transmission results also suggest that losses (particularly scattering) in the 2µm fluorescence region will be significantly lower than those at 1060 nm. With the Cr^{2+} absorption values observed in the films, the desired length of the gain medium will be less than a millimeter, so we do not anticipate that the losses will preclude observation of optical amplification in these materials. Literature reports of pure ZnS waveguides show that losses can be reduced by deposition at low temperature [26], and this suggests a way forward, although there may be a tradeoff in loss of fluorescence as the structure becomes less crystalline, affecting Cr substitution and coordination.

3.3 Structure (XRD)

The optical properties of Cr:ZnS are known to result from substitution in the Zn sites in the ZnS crystal, with the tetrahedral coordination resulting in the splitting of the $^5T_2 \rightarrow {}^5E$ levels [27]. Deposition onto unheated substrates, which results in small crystallites, is thus a somewhat unexpectedly successful technique for the fabrication of materials with a well-defined Cr^{2+} absorption band. We examined the x-ray diffraction data to determine the grain size and orientation of our films as a function of deposition conditions and Cr concentration. Using the Scherrer equation $\lambda/\beta\cos\theta$, where λ is the x-ray wavelength, β is the full peak width at half the maximum intensity (FWHM) and θ is the Bragg angle, the grain size for RT-grown films was found to be 30 nm with a standard deviation of 5 nm, which is similar to the grain size on thin (~500 nm) ET films observed by TEM [28]. For our thicker ET-grown films, the grain size was 52 nm with a standard deviation of 4 nm. Both increased substrate temperature and higher Cr concentration increase the grain size. The substitution of Cr into the lattice appears to stabilize the sphalerite crystal structure leading to larger grains.

Optical Materials EXPRESS

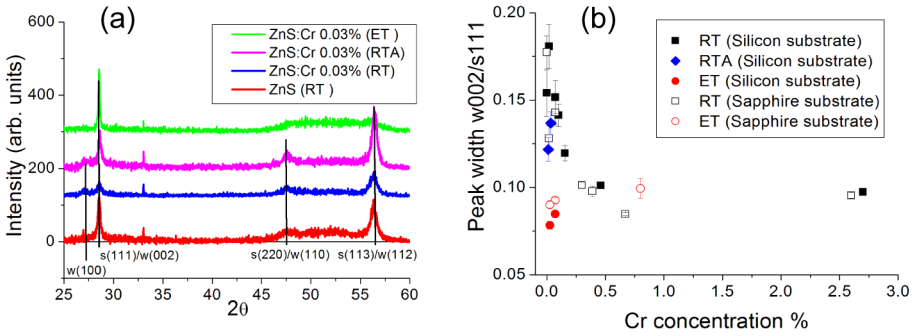

Fig. 5. (a) X-ray diffraction scans of ZnS and Cr:ZnS films deposited without substrate heating (RT), Cr:ZnS heated to 200 °C during deposition (ET) and heated to 400°C after deposition (RTA). (b) Crystalline order increases upon the addition of Cr or an increase in substrate temperature, but is not directly associated with improved fluorescence properties. Post deposition annealing enhances the (wurtzite/sphalerite) peak at 47.5 and 56.4 degrees without degrading the fluorescence.

From the XRD data, shown in Fig. 5(a), we determined that the films were polycrystalline regardless of substrate temperature, but have a strongly preferred orientation, in agreement with TEM results [28]. Determination of the crystal form is challenging due to the similarity in the lattice constants for the hexagonal (wurtzite (w)) and cubic (sphalerite (s)) forms of ZnS, but RT films have a small exclusive w(100) wurtzite peak at 2θ = 26.94, which is not observed in the ET films. For all film depositions, the largest grains were determined to be oriented in the w(002)/s(111) direction (2θ ~28.5°). Films deposited at room temperature had less order, while increasing the Cr content was seen to decrease the peak full width half maximum, as shown in Fig. 5(b), as observed with Fe:ZnS [29]. Modulation doped films had the same w(112)/s(311) dominated texture (2θ ~56.4°) as those deposited with a continuous flux, but had smaller grain sizes (~23 nm, peak width 0.39), similar to films grown on cooled substrates [26].

4. Modeling

Density functional theory (DFT) calculations were undertaken to determine the density of states (DOS) for chromium substituted for zinc in a crystalline ZnS lattice. Although absolute values obtained are typically not directly comparable with experimental data, valuable comparisons can be made between different atomic concentrations and spatial arrangements. In particular, we model the effect of a full delta-doped layer of Cr which represents a limiting case for the modulation-doped experimental results presented above.

Spin unrestricted DFT calculations were performed using the Amsterdam Density Functional BAND-structure program (BAND 2013 [30]) on a 4x3x2 repetition ($Zn_{24}S_{24}$) of the primitive cubic (sphalerite) structure. For the simulations of the homogeneous films, a Zn atom was substituted with a Cr atom, giving a structure with the chemical composition $CrZn_{23}S_{24}$, corresponding to ~2 at% Cr in the films as determined by EDX. Delta-doped films were modeled by replacing a plane of Zn with one of Cr. Initial optimization was performed using the Local Density Approximation (LDA) [31]. A second geometry optimization was then performed using the more accurate Perdew-Burke-Ernzerhof (PBE) [32] functional. A double-ζ basis set was used for all atoms. The 3d, 4s and 4p electrons of Zn and Cr were treated as valence electrons in the calculation as were the 3s and 3p electrons of S. The convergence criteria on all simulations were 1.36 x 10^{-2} eV for the energy and 2.7 x 10^{-2} eV/Å for the gradient of the energy. Figure 6 shows the results for (a) 2 at% Cr in crystalline ZnS and (b) delta-doped Cr in ZnS (16 at%), where the Fermi energy is set to be equal to zero. The sharp intra-gap Cr^{2+} levels (alpha spins) are clearly evident in the uniform (low) doping case. These calculations, which explicitly assume substitution and isolated ions, do

Optical Materials EXPRESS

not show any states that might be involved in parasitic absorption at these concentrations, from adjacent or clustered Cr, for example. The calculation for the delta-doped layers shows a small reduction and shift in the gap of the beta spin states, and a large smearing of the alpha states within the gap. These changes are due to strong interactions within the Cr layer. Although the modulation doping amplitude we introduced experimentally was not as extreme as that modeled here, the disappearance of the sharp absorption features from the intra-gap transitions is anticipated, as is an overall increase in the absorption at short wavelengths. Further modeling with a larger cell size is needed to accurately characterize the effects of modulation doping, and should include crystalline defects to simulate grain boundaries, in addition to substitutional Cr.

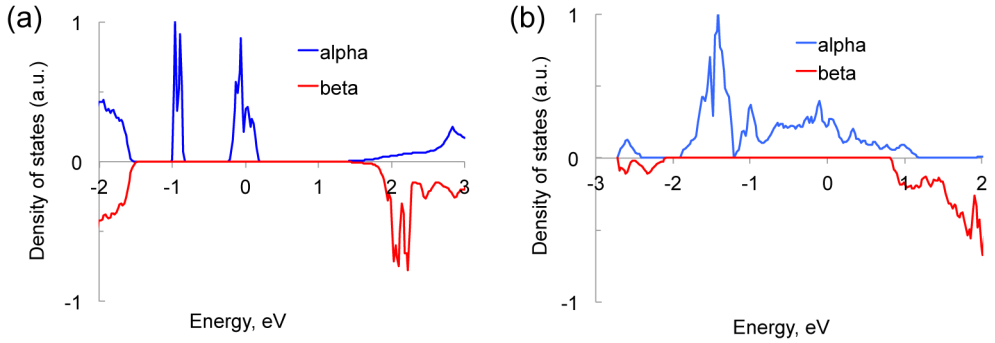

Fig. 6. Density of states from DFT calculations (a) $Cr_{.04}Zn_{.96}S$ uniform doping, and (b) delta-doped Cr in ZnS (equivalent concentration is 16 at% limited by the size of the simulation that could be run).

5. Conclusion

Films of Cr-doped ZnS deposited onto unheated substrates show promising properties for use in waveguide mid-infrared lasers. Well-isolated absorption from Cr^{2+} ions is observed for low concentrations, and absorption cross-sections appear to be comparable to those of diffusion-doped single crystals. Fluorescence yield and lifetimes are comparable to those obtained with doped single crystals [22,23], and off-resonance attenuation values are acceptably low for these to be potential gain media. Heating the substrate during deposition introduces unwanted absorption and additional scattering due to the larger grains that are formed. Modulation doping reduces the Cr^{2+} absorption, and this is likely related to reduction in the ZnS grain size during the "off" part of the cycle, or to dimensional and clustering effects which alter the band structure of the material. From these studies, the most promising route to the formation of active materials is room temperature deposition, followed by an annealing step in vacuum (RTA), where fluorescence efficiency is maintained, lifetimes are increased [23], and scattering is not excessive. These studies suggest that low Cr concentration films with uniform composition are of sufficient quality that short pathlength amplification devices may be possible in the near future.

Acknowledgments

Support for this work was provided by Norges Forskningsråd grant 219686/O70 and Notur grant number NN9291K.